Why permafrost rocks become unstable: a rock-ice-mechanical model in time and space

Journal:	*Earth Surface Processes and Landforms*
Manuscript ID:	ESP-12-0025.R2
Wiley - Manuscript type:	Special Issue Paper
Date Submitted by the Author:	n/a
Complete List of Authors:	Krautblatter, Michael; Technical University Munich, Engineering Geology Funk, Daniel; University of Bonn, Department of Geography Günzel, Friedrike; University of Brighton, School of Environment and Technology
Keywords:	mountain geomorphology, paraglacial geomorphology, rock slope stability, permafrost, rock-ice mechanics

Why permafrost rocks become unstable:

a rock-ice-mechanical model in time and space

Michael Krautblatter[a,*], Daniel Funk[b] and Friederike K. Günzel[c]

[a] *Analysis, monitoring and early warning of landslides, Technische Universität München, Munich, Germany*

[b]*Department of Geography, University of Bonn, Bonn, Germany*

[c]*University of Brighton, Brighton, UK*

* Arcisstrasse 21, 80333 München, Germany, Phone +49 89 28925866 Fax +49 89 289 25852; mail: m.krautblatter@tum.de

Keywords: mountain geomorphology, paraglacial geomorphology, rock slope stability, permafrost, rock-ice mechanics,

Abstract:

In this paper, we develop a mechanical model that relates the destabilisation of thawing permafrost rock slopes to temperature-related effects on both, rock- and ice-mechanics; and laboratory testing of key assumptions is performed. Degrading permafrost is considered to be an important factor for rock-slope failures in alpine and arctic environments, but the mechanics are poorly understood. The destabilisation is commonly attributed to changes in ice-mechanical properties while bedrock friction and fracture propagation have not been considered yet. However, fracture toughness, compressive and tensile strength decrease by up to 50 % and more when intact water-saturated rock thaws. Based on literature and experiments, we develop a modified Mohr-Coulomb failure criterion for ice-filled rock fractures that incorporates fracturing of rock bridges, friction of rough fracture surfaces, ductile creep of ice and detachment mechanisms along rock-ice interfaces. Novel laboratory

setups were developed to assess the temperature dependency of the friction of ice-free rock-rock interfaces and the shear detachment of rock-ice interfaces. In degrading permafrost, rock-mechanical properties may control early stages of destabilisation and become more important for higher normal stress, i.e. higher magnitudes of rock slope failure. Ice-mechanical properties outbalance the importance of rock-mechanical components after the deformation accelerates and are more relevant for smaller magnitudes. The model explains why all magnitudes of rock slope failures can be prepared and triggered by permafrost degradation and is capable of conditioning long paraglacial response times. Here, we present a synoptic rock- and ice-mechanical model that explains the mechanical destabilisation processes operating in warming permafrost rocks.

1 Introduction

Degrading permafrost in rock walls is considered to be an increasing hazard in alpine environments due to both, rockfall activity and slow rock deformation endangering infrastructure and potentially causing casualties (Brommer et al., 2009). The increasing importance of hydro-electric power generation and storage in high-topography settings and the trend towards high-alpine winter and adventure tourism increases the vulnerability to permafrost rock slope failure and requires improved assessment and monitoring strategies for permafrost rock walls (Haeberli et al., 1997; Messerli, 2006). Enhanced activity of rock slope failure in permafrost-affected rock slopes has been investigated at several sites in the last years. Rock-ice avalanches of bergsturz size (release volumes >1 Mm³) were documented, e.g. at Mt. Steller, Alaska ($5(\pm1)*10^7$ m³) in 2005, at Dzhimarai-Khokh, Russian Caucasus ($4*10^6$ m³) in 2002, at Mt. Steele, Yukon ($5.5*(\pm2.5)*10^7$ m³) in 2007, at Harold Price,

British Columbia ($1.6*10^6$ m^3) in 2002 and at the Brenva ($2*10^6$ m^3) and the Punta Thurwieser ($2*10^6$ m^3) in the Italian Alps in 1997 and 2004 (Bottino et al., 2002; Haeberli et al., 2004; Geertsema et al., 2006; Huggel et al., 2008; Lipovsky et al., 2008; Sosio et al., 2008). Recently, rock avalanches of a few million m^3 detached from permafrost summits such as the Bliggspitze, Kauner Valley, Austria in 2007 and in December 2011 at the Pizzo Cengalo, Bergell, Switzerland in the Alps. Enhanced activity of cliff falls (10^4-10^6 m^3), block falls (10^2-10^4 m^3), boulder falls (10^1-10^2 m^3) and debris falls (<10 m^3) was detected in several permafrost-affected rock faces (Fischer et al., 2007; Krautblatter and Dikau, 2007; Sass et al., 2007; Rabatel et al., 2008; Ravanel and Deline, 2008).

It has been postulated, that permafrost-distribution can significantly influence the stability of permafrost rock slopes and responds quickly to climatic fluctuations (Fischer and Huggel, 2008; Fischer et al., 2010). Three types of field evidence have been presented in the literature: (i) the exposure of ice at rockfall backscarps subsequent to failure (Dramis et al., 1995; Haeberli et al., 2004; Gruber and Haeberli, 2007) as well as the (ii) spatial and (iii) temporal coincidence of rock slope failure and thermal disturbances in permafrost rock walls. Huggel (2009) states that detachment zones of rock-ice avalanches indicate thermal disturbances caused by the interaction of permafrost, glacial ice, volcanic/geothermal effects and climate change. These relations were suggested for, e.g. the Kolka-Karmadon slide, Caucasus (Haeberli et al., 2003); the Iliamna avalanches, Alaska (Huggel et al., 2007); the Mt. Steller avalanche, Alaska (Huggel et al., 2008) and the Monte Rosa failure, Italy (Fischer et al., 2006). A spatial relationship between permafrost degradation and rockfall was detected by Noetzli et al. (2003) for the European Alps and by Allen et al. (2009) for the Southern Alps, New Zealand. The correspondence of annual and decadal warm periods with enhanced rockfall activity from permafrost cliffs has also been

postulated (Gruber et al., 2004; Rabatel et al., 2008). The abductive scientific reasoning of “increasing permafrost-related instability” based on the short time frame of recorded rock slope failures in high mountains is still difficult. It is, thus, important to develop a deductive systemic understanding based on the physical process linkage between permafrost degradation and rock instability (Krautblatter et al., 2012).

Permafrost dynamics influence rock slope stability due to increasing shear stresses and reducing shear resistance. Water pressure and ice segregation enhance shear forces in permafrost rocks. Fischer et al. (2010) modelled the effects of enhanced hydrostatic pressure due to a perched water level sealed by permafrost (Krautblatter and Hauck, 2007; Krautblatter et al., 2010). Ice segregation possibly acts to prepare planes of weakness by creating and extending microfractures (Murton et al., 2000; Matsuoka, 2001; Murton et al., 2006). While macrogelivation (frost wedging) is postulated to operate in rock discontinuities close to the surface (Matsuoka, 2001), microgelivation (ice segregation) could physically operate in several meters depth, where permafrost is found in Alpine environments. Upward freezing due to ice segregation could cause propagating ice-filled fractures, which may provide a slip plane during thawing (Matsuoka and Murton, 2008). However, the critical moisture content required for effective frost action (Prick, 1997) and the effectiveness of microgelevation in hard low-permeability rocks requires further research (Hall et al., 2002; Whalley et al., 2004). Degradation and warming of permafrost might also influence the shear resistance of rock masses. In constant strain experiments (where shear velocity is kept constant), the shear strength of ice-filled fractures is a function of temperature and normal stress (Davies et al., 2000; Davies et al., 2001; Davies et al., 2003; Günzel, 2008). The shear strength of the fracture declines with increasing temperature of the ice between -5 °C and 0 °C. Shear strength of the ice-filled

fractures in the presence of warm ice (-0.5 °C) is possibly less than the strength of the equivalent ice-free fracture (Davies et al., 2001). In constant strain experiments, where the shear velocity can increase freely, fracturing is also temperature-dependent but occurs due to sudden fracturing along rock-ice interfaces for low normal stress (Günzel, 2008).

However, the abrupt changes in rock-mechanical behaviour at the freezing point have not yet been integrated in such models. This is surprising since Mellor (1973) could show a drop in uniaxial compressive strength from 20-50 % and, respectively, a drop of the tensile strength varying from 15-70 % for increasing temperatures between –10 °C and 0 °C, which was later confirmed by Dahlström (1992), Lie et al. (2003) and Dwivedi et al. (1998). The most likely explanation for the strength increase at low temperature is that freezing of absorbed water in pores, micro-cracks and micro-fissures leads to an effective grouting of the rock. The abrupt changes in rock-mechanical properties (i.e. thawing could cause a drop of rock strength by 50% in a short time frame) are unparalleled by any other influence on rock strength and will have serious, presently overlooked, effects on rock instability.

Permafrost affected rock-slope failure could also be analysed and assessed within the paraglacial framework which describes the transition or adjustment of a landscape from glacial conditions to non-glacial conditions (Ballantyne, 2002; Slaymaker, 2009). Degrading permafrost in rockwalls is a possible explanation for the response time of peak landslide activity following deglaciation (Wegmann et al., 1998; McColl, 2012). Paraglacial effects on rock-slope stability could act to orchestrate landslide magnitude, frequency and location as well as their change through glacial-interglacial cycles (Korup and Clague, 2009; Korup et al., 2010; McColl, 2012). In this context, the processual and mechanical understanding of the permafrost-related failure mechanisms is also a crucial issue to decipher the

paraglacial impact among multiple other factors that influence rock slope stability (Holm et al., 2004; McColl, 2012).

This paper presents a mechanical model which combines rock- and ice mechanical concepts and parameterisation from a wide background of different related engineering subjects. The model implications are tested by laboratory experiments on untested key assumptions. The mechanical behaviour of ice-filled joints in time (response time) and space (magnitude) is hypothesized based on consequent reasoning. This paper addresses three questions:

(i) How does thawing theoretically affect rock- and ice-mechanical properties?

(ii) At what time scales (response time) and spatial scales (magnitudes) of destabilisation do rock- or ice-mechanical processes dominate instability behaviour?

(iii) How can we empirically prove the critical and novel concepts of mechanical destabilisation along rock-ice interfaces and along rock-rock contacts when thawing?

2 Deriving the rock-ice mechanical model

According to the Hoek-Brown failure criterion (Hoek and Brown, 1980) and the critical path concept (Einstein et al., 1983), rock mass failure is related to two essential processes: (i) time-dependent failure of intact rock bridges connecting non-persistent discontinuities, often conditioned by subcritical crack growth, and (ii) shear failure of discrete rock blocks overcoming frictional resistance within different material combinations (Erismann and Abele, 2001). From a mechanical point of view, the presence of permafrost can increase shear stress due to changing water pressure and cryostatic pressure, i.e. by ice segregation. Thawing permafrost can decrease shear resistance of rock masses as thawing alters the mechanical behaviour of intact rock, rock-rock contacts, rock-ice contacts and ice. In this paper, all these types of

failure are combined to derive a mechanical model for failure of frozen rock mass (Fig 1).

2.1 A preliminary rock-ice mechanical model

Fig. 1: A schematic representation of the rock-ice mechanical model

The proposed model contains shear forces acting on the potential sliding plane and the shear resistance provided by the frozen rock mass:

The shear forces are provided by:

A: Components of *gravity* and *pre-existing stresses* parallel to the shear plane

B: *Hydrostatic pressure* due to joints filled with water

C: *Cryostatic pressure* provided e.g. by ice segregation

The shear resistance of the ice-filled joint is provided by:

1: Creep and fracture of the *ice* itself

2: Failure of *rock-ice* contacts

3: Friction of rough fracture surfaces (*rock-rock contact*)

4: Fracture of *cohesive rock* bridges.

The synoptic models are based on the principle of superposition (Kemeny, 2003), i.e. the shear resistance provided by one component reduces the amount of shear stress applied to the other components. The processes act individually, in succession or in combination. The shear stress at failure is then

$$A + B + C = 1 + 2 + 3 + 4 \qquad \text{Equ. 1}$$

2.2 Permafrost induced shear stresses

2.2.1 Hydrostatic pressure (B)

The impact of permafrost on hydraulic permeability of rocks and water pressure has rarely been investigated. Pogrebiskiy and Chernyshev (1977) conducted experimental pumping and pressurization in frozen and unfrozen fissured (aperture up to 10 cm) granites. They found that the hydraulic permeability of frozen fissured rock is one to three orders of magnitude lower than the permeability of identical thawed rock. The ratio is higher for weathered rocks close to the surface with greater ice contents. Perhaps most importantly, the anisotropy of the hydraulic permeability of a rock mass strongly increases when freezing. The combination of perched groundwater and deep-reaching unfrozen fracture systems regularly causes significant problems for tunnelling structures by water inundating in permafrost rocks, e.g. reported at the Kunlun tunnel of the QingHai-Tibetian railway track, at the Zusgpitze cog wheel train tunnel (Germany), at the Aiguille du Midi (France) and at the Jungfrau (Switzerland) (Ulrich and King, 1993; Wegmann et al., 1998; Tang and Wang, 2006; Hasler et al., 2008). Enhanced water pressures due to the sealing of rock surfaces by ice can destabilise rock slopes (Terzaghi, 1962) as coupled hydro-mechanical modelling suggests for the 1988 Tschierva rock slope failure ($3*10^5$ m³) (Fischer and Huggel, 2008). The importance of pressurised water for rock slope instabilities has also been stated where outflow was observed subsequent to failure, e.g. at the scarps of Kolka-Karmadon and Mt. Steller (Haeberli, 2005; Gruber and Haeberli, 2007; Huggel et al., 2008). However, no detailed empirical quantitative studies exist on repository and water pressure effects in permafrost rock walls.

2.2.2 Cryostatic pressure and ice segregation (C)

Ice pressure build-up can derive from volumetric expansion of in situ water (Hall et al., 2002; Matsuoka and Murton, 2008) and ice segregation (Walder and Hallet, 1985; Hallet, 2006; Murton et al., 2006). In the laboratory, open systems allow water migration and support ice segregation, while closed water-saturated systems favour volumetric expansion (Matsuoka, 1990). Ice pressure by volumetric expansion could theoretically cause stresses up to 207 MPa (Matsuoka and Murton, 2008). Ice pressure can be relaxed through ice deformation and ice expansion into free spaces and ice extrusion (Davidson and Nye, 1985; Tharp, 1987). These effects can lead to stress reduction and contraction of frozen ice-filled rock samples in the long-term (Matsuoka, 1990). Ice segregation along temperature gradients in fissured natural bedrock will cause cryosuction up to several MPa (Walder and Hallet, 1985; Murton et al., 2006; Matsuoka and Murton, 2008) and is likely to generate more or less persistent elevated levels of cryostatic stress in permafrost rocks. Effective ice segregation requires a temperature gradient for sub-zero temperatures ideally from -3 to -6 °C, water supply and an inter-crack pressure slightly above the tensile strength of rock (Hallet et al., 1991). These conditions frequently occur at the base of the active layer above the permafrost table (Hallet et al., 1991; Murton et al., 2006). Heaving pressures of 20 to 30 MPa exceed the tensile strength of even strong rocks and can cause crack propagation (Hallet et al., 1991). For potential shear planes at greater depths (>10 m) below ground, reduced temperature gradients and water availability, combined with increased normal stress effectively counteract the formation of ice and squeeze out ice between protruding rock-rock contacts over time and hence reduce the importance of ice segregation. This so-called “shut off pressure” for ice segregation at normal stresses higher than 200 kPa (equivalent to 8

m rock overburden) has been observed and described by Clark & Phillips (2003), Nixon (1982) and Konrad & Morgenstern (1982).

2.3 Permafrost induced shear resistance

2.3.1 Creep and fracture of ice in rock joints (1)

Several studies show that most subsurface fractures in Alpine permafrost bedrock are ice-filled (Körner and Ulrich, 1965; Haeberli, 1992; Ulrich and King, 1993; Gruber and Haeberli, 2007). This is not surprising since alpine bedrock is mostly water-saturated (apart from the surface) and ice acts to attract water by cryosuction (Sass, 2005). Ice does not deform in a purely elastic, viscous or plastic way and, thus, does not readily lend itself to classical engineering analysis in terms of “strength” and “failure” (Sanderson, 1988). However, these terms have been used for a straightforward characterisation of ice-mechanical properties (Sanderson, 1988; Paterson, 2001). Hereafter, ice properties will be separated in ductile behaviour due to elastic and plastic creep deformation without fracture and fracturing due to brittle or brittle-ductile behaviour.

It is assumed that ice-filled discontinuities react according to stress-strain behaviour of polycrystalline ice. The deformation of pure ice is characterized by four phases: Elastic deformation (1) that is followed by plastic deformation, firstly at a decreasing rate (2, primary creep), then at a constant rate (3, secondary creep) and finally at an increasing rate (4, tertiary creep) (Budd and Jacka, 1989). Mostly secondary creep and tertiary creep occur at speeds relevant for active mass movements. The flow relation (Glen’s Law) for secondary creep relates the shear strain rate ε'

$$\varepsilon' = A\tau^n \qquad \text{Equ. 2}$$

to the shear stress τ, where the Arrhenius factor *A* depends mainly on ice temperature, crystal size and orientation, impurity content and water content in the ice (Paterson, 2001). The exponent n is usually assumed to be 3 in ice–sheet modelling at axial stresses between 0.2 and 2 MPa (Paterson, 2001; Schulson and Duval, 2009). Crystal orientation, impurity content and shear stresses remain more or less constant over short timescales. In contrary, ice temperature and water content in mass movement systems are subject to major annual and interannual changes. The factor *A* can be approximated by the Arrhenius relation, which can be used at all temperatures (Paterson, 2001). For temperatures above -10 °C *A* can be approached by

$$A = A_0 \exp\left(-\frac{Q}{RT}\right) \approx A_0 \exp\left(-\frac{16700}{T_k}\right) \quad \text{Equ. 3}$$

where A_0 is independent of temperature, R is the universal gas constant and Q is the activation energy (Weertman, 1973). The T-dependency of *A* is partly counteracted by the T-dependency of *Q* which increases at T > -10 °C (Schulson and Duval, 2009). But this seems to be negligible, since empirical values show a strong increase of *A* with T from $4.9*10^{-6}$ [s^{-1} $(kPa)^{-3}$] at -10 °C over $24*10^{-6}$ [s^{-1} $(kPa)^{-3}$] at -2 °C to $68*10^{-6}$ [s^{-1} $(kPa)^{-3}$] at 0 °C (Paterson, 2001). A_{0t} for tertiary creep

$$A_{0t} = (3.2 + 5.8W) \times 10^{-15} (kPa)^{-3} s^{-1} \quad \text{Equ. 4}$$

can be related to the water content W [%]. Paterson (2001) states that -2 °C is the lowest temperature at which a sufficient amount of water exists in the ice to affect the stress-strain behaviour. Equ. 3 and Equ. 4 show, that both, ice temperature and water content play a dominant role for the mechanical behaviour of ice-filled joints at temperatures close to 0 °C. Assuming a moderate water content of 0.6 % at 0 °C, the creep rate at 0 °C is three times the rate at -2 °C (Paterson, 2001).

Exceeding the thresholds for stress, strain or strain rate (for uniaxial compression this is 5-10 MPa, 1 % and 10^{-3} s^{-1}, respectively), ice deforms in a brittle and ductile-brittle manner after seconds to minutes until complete fracture occurs (Sanderson, 1988). Tensile fracturing can already occur at 1-2 MPa. As 1 MPa equals the normal stress of 40 m rock overburden, one could expect that fracturing phenomena may only influence high-magnitude rockslides. However, stress is very unequally distributed in unstable rocks (Eberhardt et al., 2004) and thus tensile and compressive stresses in the range of 1 MPa (equals gravitational force of 10 kg on a cm^2) can exist locally even in rockslides of a few meters thickness. On the other hand, Renshaw & Schulson (2001) and Sanderson (1988) showed that both, rock and ice materials tend to react rather ductile than brittle under high confinement.

2.3.2 Failure of rock-ice contacts (2)

For a lower thickness of the detachment layer and for high deformation rates, the detachment of the rock-ice interface is more likely than the failure of the ice itself. Shearing experiments using concrete-ice samples under constant strain show that for normal load up to ca. 300 kPa (equivalent to 12 m rock overburden), the failure occurs at the concrete-ice interface and not within the ice (Günzel, 2008). In constant stress experiments, where the rate of deformation can accelerate freely, all experiments simulating up to 630 kPa (25 m overburden) caused a detachment of the rock-ice interface (Günzel, 2008). Thus, we used the constant stress experiments as a representation of rock-ice detachment processes; the development of the formula dependent on normal load and temperature is described in a section 4.1..

2.3.3 Friction along rock fractures (rock-rock contact) (3)

The influence of ice and low temperatures on the frictional behaviour of rock fractures has not been investigated yet. However, a significant change must be expected when combining the rock friction theory (Equ. 5) with empirical findings on the rapid change of intact rock strength at the freezing point (see below). The peak shear strength of separated rock blocks along a rough joint can be expressed as

$$\tau_p = \sigma' \tan\left(JRC \times \log_{10}\left(\frac{\sigma_u}{\sigma'} \right) + \varphi_r \right) \qquad \text{Equ. 5}$$

where τ_p is the peak shear strength, σ' is the effective normal stress, JRC is the joint roughness coefficient, σ_u is the joint wall compressive strength and φ_r is the residual friction angle of a smooth unweathered rock surface (Barton and Choubey, 1977).

For saturated intact rock, Mellor (1973) could show a drop in uniaxial compressive strength from 20 % (Barre Granite, porosity p = 1.2 %) to 50 % (Berea Sandstone, p = 20 %) and, respectively a drop of the tensile strength varying from 15 % to 70 % for increasing temperatures between –10 °C and 0 °C (see also Dahlström, 1992; Dwivedi et al., 1998; Li et al., 2003). The loss of strength correlates with rock porosity and water content, is more pronounced for tensile strength than for compressive strength and corresponds to changes in Poisson's ratio, Young's modulus and the joint stiffness (Inada and Yokota, 1984; Glamheden, 2001).

The increase of the uniaxial compressive strength (σ_u in Equ. 5) under frozen conditions increases the peak shear strength due to an inhibited shearing of asperities. Thus, the friction of rock joints is presumably higher under frozen conditions than under unfrozen conditions even for rock-rock contacts without ice intercalation. This effect should be more pronounced for rougher fractures with a higher JRC.

2.3.4 Fracture of intact rock bridges (4)

The susceptibility of rock bridges to fracturing will increase in thawing rock. Failure of intact rock bridges occurs due to both critical and subcritical crack growth (Atkinson, 1982). Critical crack growth occurs when the stress intensity factor K exceeds the fracture toughness K_C (Irwin, 1958). Subcritical crack growth occurs even when $K_C < K$ and is time-dependent. Conceptualising an individual rock bridge as a patch of intact material between two coplanar cracks, K_{II} can be incorporated in the cohesion term of the Coulomb failure criterion (Kemeny, 2003)

$$\tau_p = \frac{K_{IIC}\sqrt{\pi a}}{2w} \quad with \quad K_{II} = \frac{\tau 2w}{\sqrt{\pi a}} \quad and \quad K_{II} = K_{IIC} \quad for \quad \tau = \tau_p \qquad \text{Equ. 6}$$

where K_{IIC} is the Mode II fracture toughness, K_{II} is the Mode II stress intensity factor, a is the half width of the rock bridge, $2w$ is the bridge-to-bridge spacing, and τ_p is the peak shear strength.

Freezing of water-saturated intact rock enhances the fracture toughness. Fracture toughness increases by 8 % for dolerite (p = 0,5 %) and by 37 % for fine-grained sandstone (p = 5 %) samples when freezing to –10 °C dependent on moisture content and temperature (Dwivedi et al., 1998; Dwivedi et al., 2000). Pressure-maintained solutions at the crack tips in greater depths promote chemical activity and possibly enhance fatigue effects when frozen rock is thawing (Whalley, 1982). Studies on P-wave velocity suggest that the most pronounced change in fracture toughness occurs close to the equilibrium freezing point as has been shown for compressive and tensile strength in earlier studies (Mellor, 1973). P-wave velocity is the highest correlated proxy to Mode I fracture toughness (R^2 of 0.8) and Mode I and II fracture toughness correlate closely (Chang et al., 2002). P-wave velocities of 22

arctic and alpine low-porosity bedrock samples were shown to increase by a factor of 1.1-2.6 subsequent to freezing mostly between the equilibrium freezing point with a mean of -0.5 °C and -3 °C (Draebing and Krautblatter, 2012) .

3 The rock-ice mechanical model

The frictional resistance of rock can thus be formulated as:

$$\left|\tau_p\right| = \varepsilon_w / A_0 \exp\left(-\frac{16700}{T_K}\right)$$ Secondary creep of ice (Equ. 2 + 3)

$$+\left(-144 * T_C + 0.42 * \sigma' + 41.3\right)$$ Failure of rock-ice contact (Equ. 7 + 8, see 4.1.3)

$$+\sigma' \tan\left(JRC * \log_{10}\left(\frac{\sigma_u}{\sigma'}\right) + \varphi_r\right)$$ Friction of rock-rock contacts (Equ. 5)

$$+\frac{K_C\sqrt{\pi a}}{2w}$$ Fracturing of rock bridges (Equ. 6)

where the critical fracture toughness K_c, the uniaxial compressive strength σ_c and temperature T_c [°C] and T_K [K] are the sensitive parameters to warming. This equation explains why rock fracturing, rock friction, creep of ice and failure of rock ice contacts will heavily respond to changes of K_c up to 40 % and to changes of σ_c up to 50 % (Mellor, 1973; Dwivedi et al., 2000) and temperature changes (T_C and T_K) when thawing. This basic equation could then be adapted to specific conditions. Adaptations could be necessary (i) to reflect the geometry and failure mode of rock bridges, (ii) and to specify the type of deformation of the ice inside the rock fracture. Moreover, the equations reflecting friction and failure of rock-ice contacts need to be generalized as they yet reflect only certain types of contact geometries and mechanical behaviour.

3.1 Instability in time: initiation and acceleration of instability

Assuming that initial deformations destructing rock bridges are (i) too slow to cause ice fracture and failure of rock-ice contacts (strain rate threshold see Sanderson, 1988) and (ii) are too slow to allow creep deformation of ice take up significant amounts of stress (strain-dependent shear resistance Equ. 2), the failure criterion for the preparation of new sliding planes is

$$|\tau| = \sigma' \tan\left(JRC * \log_{10}\left(\frac{\sigma_u}{\sigma'}\right) + \varphi_r \right) \quad \text{(Equ. 5)}$$

$$+ \frac{K_C \sqrt{\pi a}}{2w} \quad \text{(Equ. 6)}$$

where σ_u and K_c decrease significantly between –5 °C and 0 °C. Thus, slow initial destabilisation is likely to occur due to changes in rock friction and fracturing. The failure of single rock bridges will create a positive feedback as more shear stress is then applied to the remaining rock bridges. After the destruction of cohesive rock bridges, the acceleration of dislocations along the thawing fracture is governed by

$$|\tau| = \varepsilon_w / A_0 \exp\left(-\frac{16700}{T_K}\right) \quad \text{(Equ. 2 + 3)}$$

$$+ \left(-144 * T_C + 0.42 * \sigma' + 41.3\right) \quad \text{(Equ. 7 + 8)}$$

$$+ \sigma' \tan\left(JRC * \log_{10}\left(\frac{\sigma_u}{\sigma'}\right) + \varphi_r \right) \quad \text{(Equ. 5)}$$

where an increase in T_K decreases the amount of shear stress that is “absorbed” by the creep deformation of ice. Thus, faster deformations are controlled by the creep of ice, the propensity for rock-ice detachments and the friction of rock-rock contacts. The amount of stress absorbed by the total friction at rough fracture surfaces

decreases with warming due to declining compressive rock strength. An increase of T_c facilitates the failure of ice in rock joints. The warming of permafrost rock masses between -5 °C and 0 °C promotes both, the slow progressive development of new shear planes, controlled by rock mechanics, and, subsequently, the accelerating failure along predefined sliding planes that is increasingly controlled by ice-mechanics.

3.2 Instability in space: the magnitude effect

Fig. 2: The efficiency of shear force and shear resistance with depth of the shear plane.

The spatial differentiation of processes controlling rock slope stability, i.e. with normal stress, is a classical concept in rock instability research (Terzaghi, 1962; Whalley, 1984). The efficiency of all processes outlined above varies with normal stress (Fig. 2). Some processes are more pronounced for shallow (low-magnitude) rock slope failures, others are more pronounced for deep-seated (high-magnitude) rock slope failures. While water pressure exists at all depths, there is a “shut off” pressure for ice segregation that is approximately equivalent to 20 m rock overburden (Nixon, 1982; Clark and Phillips, 2003). The same has been reported for rock-ice detachments. In constant stress experiments, all experiments simulating up to 630 kPa (25 m overburden) caused a detachment of the rock-ice interface (Günzel, 2008). Rock-ice detachments and fracturing of ice itself are suppressed in favour of creep of ice at greater depths, i.e. higher confining pressures (Sanderson, 1988). In contrast, the contribution of rock friction and fracturing to the overall stability tends to increase with higher normal stress (Section 4.3.2). Thresholds needed for the initiation of fracturing

along critical paths are often not reached in shallow depths (Eberhardt et al., 1999). In conclusion, ice-mechanical processes are important for shallow (low-magnitude) rock slope failure with a depth of the shear plane below 20 m, while rock-mechanical processes might dominate deep seated (high-magnitude) rock slope failure in warming permafrost rocks close to thawing.

4 Validation of the rock-ice mechanical model – laboratory experiments

The rock-ice mechanical model described above is derived from empirical studies on the effect of ice on rock mechanical parameters and their application on established rock- and ice-mechanical concepts on friction and fracturing. Laboratory experiments were conducted to validate the general performance of frictional und fractional processes in a thawing rock fracture.

4.1 Shear strength of rock-ice interfaces

Some of the findings reported here were described in a conference paper (Günzel, 2008). However, the exact layout and the development of a general temperature and stress-dependent failure criterion has not been reported before.

4.1.1 Methods

Shear experiments were carried out under constant strain and constant stress, which represents a boundary condition similar to the constant stress situation in natural slopes (Günzel, 2008). To simulate the natural and reproducible roughness of the rock joints, samples were made of high-strength concrete (Densit Ducorit D4) with a

regular saw-tooth surface. The saw-teeth had an angle of 20° and amplitude of 1.0 mm (Fig. 3).

Fig. 3: Dimensions of the saw-tooth surface

Two sample types were used to simulate different infill thickness: concrete-ice samples and sandwich samples. The concrete-ice samples consist of a concrete block with saw-tooth surface overlain by an equally thick ice block. This sample type simulates an ice filled joint with the ice thickness being much larger than the amplitude of the surface roughness. The concrete-ice samples are prepared by placing the concrete block into a mould filled with water and allowing it to freeze.

The sandwich samples consist of two saw-tooth concrete blocks with a 1 mm thick layer of ice in between. This sample type simulates an ice thickness equal to the amplitude of the surface roughness. For preparation, the two concrete blocks are immersed in water in a mould (Fig. 4a). A bolt is glued to the top block which passes through a bar across the mould. The top block is then lifted by turning the nut against the bar while the movement is measured with an LVDT (Linear variable differential transformer). After that the surplus water on top of the sample is drained and the sample is frozen.

Temperatures inside the sample was measured with a thermocouple cast into the concrete block; the sensitive tip is located a small cavity in the centre of the sample. Tests were carried out in a 60 mm × 60 mm direct shear box modified with a pulley system and weights to apply a constant shear stress to the samples (Fig. 4b). Normal stress between 135 and 620 kPa were also provided by hanging weights. Horizontal and vertical displacements were measured with LVDTs, the shear stress was measured with a load cell. After applying both normal and shear stress the sample

temperature was kept below -4 °C in a cold room for several hours before increasing it at a rate of approximately 0.3 °C per hour until the sample failed.

Fig. 4: a) Preparation of sandwich sample; **b)** Schematic overview over experimental set-up of the constant stress tests

4.1.2 Results

The results for concrete-ice samples and sandwich samples are very similar and we will hereafter refer to concrete ice samples results as shown in Fig. 5 (plotted against time) and Fig. 6 (plotted against horizontal displacement). The decrease of stress during the test is due to friction in the pulley system and the apparent change of the rate of temperature increase in Fig. 6 is due to the increasing rate of horizontal deformation immediately before failure of the sample.

The horizontal displacement during the constant stress tests was considerably slower than during the constant strain tests, it varied between 0.002 mm/hr and 0.06 mm/hr. The deformation rate increased with increasing shear stress but no significant change could be observed for increasing normal stress or temperature. The horizontal displacement at failure was between 1.5 mm and 2.5 mm, similar to the displacement at failure of the constant strain tests. The vertical displacement decreased with increasing normal stress.

Fig. 5: Results of a constant stress experiment (concrete-ice sample, normal stress = 207 kPa) plotted against time.

Fig. 6: Results of a constant stress experiment (concrete-ice sample, normal stress = 207 kPa) plotted against horizontal displacement.

4.1.3 Discussion

Fig. 7: Shear stress at failure plotted against failure temperature for constant-stress tests with concrete-ice samples.

Fig. 7 shows the shear stresses at failure plotted against the temperature at failure for normal stresses between 136 kPa and 633 kPa. In constant stress experiments, the shear stress at failure τ_f is not a peak shear stress τ_p in the strict sense. A clear linear relationship can be observed between the shear strength and the failure temperature for each normal stress value. The slopes of the linear relationships are very similar with values between -126 and -151 kPa/°C. In Fig. 7 the trend-lines were forced to the same average slope of -144 kPa/°C slightly reducing the average correlation coefficient to 0.94-0.95. The trend-lines were the basis for Fig. 8 which shows the linear relationship of the shear stress vs. normal stress at 0 °C. The only exception is the value for the lowest normal stress (136 kPa).

Fig. 8: Linear relationship of shear stress at failure vs. normal stress for constant stress tests for 0°C.

The linear relationships in Fig. 7 and Fig. 8 are now used to formulate a general equation for the shear strength of the rock-ice contact:

$$\tau_f = 144 * T_C + \tau_0 \qquad \text{Equ. 7}$$

where T_C (°C) is the is the temperature of the ice at failure, τ_f is the shear stress at failure and τ_0 is the shear strength at 0 °C. The value of τ_0 is approximated from Fig. 8:

$$\tau_0 = 0.42 * \sigma' + 41.3 \quad \text{Equ. 8}$$

4.2 Frictional strength of rock-rock surfaces

Changes in frictional properties of frozen rocks have not been mentioned in the literature before but can be deduced from theoretical considerations provided in Section 2.3.4. Here, we provide a new lab experiment to test the general assumption based on 40 carefully designed friction tests in a freezing chamber.

4.2.1 Methods

Three direct shear tests series on rock samples of two different lithologies were conducted. These test whether peak shear strength of a rock joint at a given roughness is higher under frozen conditions than under unfrozen conditions even if no ice is present in the joint; and determine the controlling factors of the shear strength. These benchmark tests are preliminary and intend to validate the general assumption of Equ. 5.

Experimental setup

Samples of two similar lithologies (Wetterstein limestone [L1, L2] and Wetterstein dolomite [D1]) were taken from the Zugspitze permafrost summit (Germany/Austria). These have a homogeneous, isotropic fine-grained texture which predestines them for rock-mechanical experiments similar to the Solnhofen limestone (Miller, 1961). Three pairs of cuboid samples were produced with a thickness of 10-15 mm and a shear plane of 35 * 35 mm. Samples were fitted tightly into a customised steel specimen holder of the shear frame. The specimens were saturated under atmospheric pressure to reproduce natural conditions (Krus, 1995; Sass, 2005). The

roughness of the shear plane was generated using an abrasive paper with a grit of 24 grains per inch similar to joint roughness coefficients also found in actively displacing fractures at the Zugspitze. The roughness was generated unidirectional which results in an irregular saw tooth pattern with a maximum amplitude and wave length equivalent to the paper grain size of 764 µm. The specimens were cleaned after sanding in an ultrasonic bath to free them from loose particles.

For the shear test, a modified direct shear device providing a maximum shear load of 5 kN was used. The direct shear box is placed in a thermally isolated freezing chamber. Cooling is provided by a plate cooler which is controlled by an external Pt 100 temperature sensor placed close to the sample. The cold air is removed from the cooler plate using a 3-channel enforced chilling system and transported to the thermally isolated shear device via a high-performance ventilation system. Within the shear box chamber, minimum air temperatures below -10 °C can be achieved and the sample temperature can be controlled with an accuracy of 0.5 °C. The specimen was sheared at a given normal load under frozen and subsequently under unfrozen conditions at a constant velocity of 1 mm/hr. Shearing was stopped after a shear displacement of at least 6 mm. Between the tests, each specimen was re-saturated and initial roughness was reconditioned. Frozen tests were conducted at a specimen temperature at –4.5 (±0.5) °C to guarantee the frozen state of the specimen. A drying agent was applied to extract the moisture from the air inside the shear frame chamber. This method prevented the formation of an ice layer on the shear plane. The normal load of 74 and 1333 kPa was applied after freezing to avoid the crushing of asperities by uniaxial compression before the desired testing conditions were attained.

4.2.2 Results

More than 40 shear tests à 6 to 10 hrs were conducted using three different sample-pairs. The shear test results from the three test series are visualized by *shear strength – normal stress* diagrams in Fig. 10a (D1 – dolomite), Fig. 10b (L1 – limestone) and Fig. 10c (L2 – limestone). For all three test series the angle of friction is higher for frozen tests ($\varphi_{\blacktriangle}$) than for unfrozen tests ($\varphi_{\blacksquare}$). The difference in the angle of friction between frozen and unfrozen tests is 4.6° for specimen L1, 6.4° for specimen L2 and 4.4° for specimen D1. It is remarkable that for all three test series there is practically no difference in shear strength between frozen and unfrozen tests below normal stresses of about 400-600 kPa which corresponds to the expectations according to the dilatation–shearing of asperities transition developed by Patton (1966). An increase of shear strength due to freezing is obvious for higher normal stresses (~500-1400 kPa) and the mean absolute peak values of frozen rock friction increase as much as 65 to 160 kPa (14-17 %) in comparison to unfrozen values.

Fig. 9a-c: Peak shear strength – normal stress relationships for direct shear tests on the dolomite sample (D1) and limestone samples (L1, L2) performed with constant velocities.

4.2.3 Discussion

The *shear strength – normal stress* relationships display a clear linear behaviour (R^2 > 0.94) and a clear difference between frozen and unfrozen test results above 500 kPa for all three test series. Even though the differences are not very large, they are consistent and, given to the small roughness of the samples, they perform in the range of expected values. To account for the accurate description of the friction angle, we carefully discuss all potential sources of noise:

3.2.3.1. Potential errors

Machine errors: Changes in frictional properties of the shear machine due to temperature changes and freezing were evaluated using dummy samples prior to the experiments. This error was systematically corrected in all measurements.

Specimen errors: For the entire test series the same specimens were used with the same orientation within the shear frame to reduce the effects of material inhomogeneity and variances in sample production. The grain size of the sanding paper and the orientation of the roughness pattern were kept constant to omit the effect of inconsistent roughness geometry. While a perfect replication of the initial geometry is impossible the mean roughness geometry is identical for all tests and the spacing of asperities remains constant (764 µm).

Ice influence: A drying agent was used to extract moisture from the experimental set-up to guarantee that no ice develops on the shear plane. Furthermore, samples were checked after each test for ice-bonding and tests were repeated when an ice layer was observed on the shear plane.

3.2.3.2. Explanatory power

Role of roughness: The failure mode of a joint is always a mixture of dilation and shearing of asperities (Barton and Choubey, 1977). Shearing is enhanced when the relation of the joint wall compressive strength (σ_u) to the effective normal load (σ') (Equ. 5) is reduced. This reduction can be very sudden due to a change in the thermal state from unfrozen to frozen (Mellor, 1973). A decrease in shear strength due to thawing can only be caused by the enhanced shearing of asperities, as this is the only rock-mechanical change in the system [see 2.3.3]. Given the small scales of roughness used in the tests, we expected small but well reproducible changes in friction. This is due to the high statistical number of small asperities (spacing 764 µm)

that are susceptible to shearing along the joint. At a higher roughness, the thawing decrease in friction is expected to be more significant, but more difficult to reproduce in the laboratory.

Role of compressive strength: The effect of strength increase due to freezing is dependent on the number of flaws which can be sealed (Inada and Yokota, 1984; Glamheden, 2001). Consequently, for highly -porous or stressed asperities enhanced failure is expected. In the present experiments, we used low-porous rock samples (~2 % effective porosity). A moderate decrease of intact rock strength when thawing is expected similar to the reported change in fracture toughness < 37 % for a 2.7 % porosity limestone (Dwivedi et al., 2000).

These theoretical considerations support the test results which are in the range of expected values. We expect an elevated decrease of friction due to thawing for higher roughness, a higher degree of fissuring or a higher porosity. We think that the present friction data provides a good indication that Equ. 5 is an appropriate model for the mechanical description of thawing rock fractures, but this statement can be asserted by a broader experimental test-series in the future.

4.3 Discussion of the rock-ice mechanical model

The rock-ice mechanical model presented above is based on fundamental rock- and ice-mechanical principles and experimental testing of geotechnical properties under frozen conditions. The novel preliminary but comprehensive model criterion covers the most important mechanical processes controlling rock-slope stability.

For instance, infilling in rock discontinuities may control the shear strength when the infill thickness-roughness ratio becomes critical (Goodman, 1970; Indraratna et al., 2005). Thus, grain size distribution of the filling material and failure of the infill-rock

interface become important (de Toledo and Freitas, 1993; Indraratna et al., 2005). Günzel (2012) shows that rock joints with frozen (sandy) infill material indicate higher peak shear strength and a stronger temperature-dependency than observed for pure ice. Arenson et al. (2007) concluded that the volumetric ice content and strain rate are key factors for the strength characteristics of dirty ice. Ice bonding between particles provides cohesion resulting in a stiffer behaviour at the beginning of shearing at low confining stress. At strain rates high enough to prohibit healing of the ice matrix, the residual shear strength of frozen soil is similar to that of unfrozen soil. At strain relaxation, the ice-bonding heals itself due to refreezing and causes a strengthening of the sample (Arenson and Springman, 2005).

The rock-ice mechanical model might also contribute to a different understanding of the paraglacial concept (Ballantyne, 2002). While the impact of climate signals on pre-existing stress-patterns due to regional tectonic input is increasingly disregarded (McColl, 2012), new explanations are needed for the long response time (millennia) between Lateglacial glacier retreat and the culmination of large rock slope failures in Alpine regions (Prager et al., 2008). Our model is capable of explaining both, (i) the slow external control, conditioned by the gradual and presumably cyclic warming/thawing of Alpine rock walls over millennia in the Lateglacial/Holocene period (Noetzli and Gruber, 2009), and (ii) the slow internal response, determined by the gradual decrease in mechanical strength which onsets long-term fracture propagation and acceleration of rock slope failure. Perhaps most important, it explains why all magnitudes of rock slope failures can be prepared and triggered by permafrost degradation, why higher magnitudes were ruled out in previous ice-mechanical attempts. The rock-ice mechanical model is a step towards the framework demanded by Whalley (1984) for a combined mechanical, geotechnical and geomorphological stability analysis and process study amalgamating spatial,

temporal and magnitude effects together reminiscent of combined effects of rock and ice mechanics.

5 Conclusions

A failure criterion for permafrost rock masses has been developed which represents creep of ice in an ice-filled rock joint, failure of rock-ice contacts, friction of rough fracture surfaces, and fracture of cohesive rock bridges. Analysing the temporal and spatial dimensions of the relevant processes, several spatial and temporal implications for rock slope deformations due to thawing permafrost can be suggested:

During slow deformations along critical paths with cohesive rock bridges, warming influences the total friction and the fracture toughness of rock bridges (Model I). During fast deformations along existing shear planes, warming influences the creep of ice, the propensity of rock-ice detachments and total friction (Model II). Model I accounts for slow subcritical destabilisation of degrading permafrost rock slopes over months to millennia, subsequent to the warming impulse (relaxation time). Model II explains the rapid response of rockslides to warming that occurs along existing shear planes over days to months (reaction time). High magnitudes (>20 m thick detachment layer) can only be explained by rock-mechanical changes (Model I) while for smaller magnitudes ice-mechanical processes might become more important (Model II).

Essential elements of this failure criterion could be validated by new laboratory experiments on joint friction under frozen conditions. It could be demonstrated for the first time that friction of rock joints without ice infill decreases by approximately 15 % subsequent to thawing. Furthermore, we develop a laboratory-based model that

relates rock-ice detachments in ice filled joints to normal stress and temperatures between -5 and -0.5 °C.

A quantitative rock-ice-model is presented that relates the destabilisation of thawing permafrost rocks to temperature-related effects on both, rock- and ice-mechanics and shows their applicability in time and space. Our model is capable of explaining the long paraglacial response time to cyclic warming of Alpine rock walls over millennia in the Lateglacial and Holocene.

6 Bibliography

Allen, S.K., Gruber, S., Owens, I.F., 2009. Exploring Steep Bedrock Permafrost and its Relationship with Recent Slope Failures in the Southern Alps of New Zealand. Permafrost and Perigl. Process. 20, 345–356.

Arenson, L., Springman, S., 2005. Triaxial constant stress and constant strain rate test on ice-rich permafrost samples. Can. Geotech. J. 42, 412-430.

Arenson, L., Springman, S., Sego, D.C., 2007. The rheology of frozen soils. Applied Rheology 17, 1-14.

Atkinson, B.K., 1982. Subcritical crack propagation in rocks: theory, experimental results and applications. J. Structural Geology 4, 41-56.

Ballantyne, C.K., 2002. Paraglacial geomorphology. Quaternary Science Reviews 21, 1935-2017.

Barton, N., Choubey, V., 1977. The shear strength of rock joints in theory and practice. Rock Mechanics 10, 1-54.

Bottino, G., Chiarle, M., Joly, A., Mortara, G., 2002. Modelling rock avalanches and their relation to permafrost degradation in glacial environments. Permafrost and Periglac. Process. 13, 283-288.

Brommer, C., Phillips, M., Keusen, H.-R., Teysseire, P., 2009. Bauen im Permafrost; Ein Leitfaden für die Praxis. Eidg. Forschungsanstalt für Wald, Schnee und Landschaft WSL, Birmensdorf.

Budd, W.F., Jacka, T.H., 1989. A review of ice rheology for ice-sheet modeling. Cold Regions Science and Technology 16, 107-144.

Chang, S.-H., Lee, C.-I., Jeon, S., 2002. Measurement of rock fracture toughness under modes I and II and mixed-mode conditions by using disc-type specimens. Engineering Geology 66, 79-97.

Clark, J.I., Phillips, R., 2003. Centrifuge modelling of frost heave of arctic gas pipelines. In: Phillips, M., Springman, S., Arenson, L. (Eds.), Permafrost - 8th International Conference. AA Balkema, Zurich, Switzerland.

Dahlström, L.-O., 1992. Rock Mechanical Consequences of Refrigeration. Chalmers University of Technology, Göteborg.

Davidson, G.P., Nye, J.F., 1985. A Photoelastic Study of Ice Pressure in Rock Cracks. Cold Reg Sci Technol 11, 141-153.

Davies, M.C.R., Hamza, O., Harris, C., 2001. The effect of rise in mean annual temperature on the stability of rock slopes containing ice-filled discontinuities. Permafrost and Perigl. Process. 12, 137-144.

Davies, M.C.R., Hamza, O., Harris, C., 2003. Physical modelling of permafrost warming in rock slopes. In: Phillips, M., Springman, S., Arenson, L. (Eds.), 8th Int. Con. on Permafrost. Balkema, Zürich, pp. 169-174.

Davies, M.C.R., Hamza, O., Lumsden, B.W., Harris, C., 2000. Laboratory measurements of the shear strength of ice-filled rock joints. Annals of Glaciology 31, 463-467.

de Toledo, P.E.C., Freitas, M.H., 1993. Laboratory testing and parameters controlling the shear strength of filled rock joints. Geotechnique 42, 1-19.

Draebing, D., Krautblatter, M., 2012. P-wave velocity changes in freezing hard low-porosity rocks: a laboratory-based time-average model. The Cryosphere.

Dramis, F., Govi, M., Guglielmin, M., Mortara, G., 1995. Mountain Permafrost and Slope Instability in the Italian Alps: the Val Pola Landslide. Permafrost and Perigl. Process. 6, 73-82.

Dwivedi, R.D., Singh, P.K., Singh, T.N., Singh, D.P., 1998. Compressive strength and tensile strength of rocks at sub-zero temperature. Indian J. Eng. Mat. Sc. 5, 43-48.

Dwivedi, R.D., Soni, A.K., Goel, R.K., Dube, A.K., 2000. Fracture toughness of rocks under sub-zero temperature conditions. Int. J. Rock Mech. & Mining Sciences 37, 1267-1275.

Eberhardt, E., Stead, D., Stimpson, B., 1999. Quantifying progressive pre-peak brittle fracture damage in rock during uniaxial compression. Int. J. Rock Mech. Min. Sci. 36, 361-380.

Eberhardt, E., Spillmann, T., Maurer, H., Willenberg, H., Loew, S., Stead, D., 2004. The Randa Rockslide Laboratory: Establishing brittle and ductile instability mechanisms using numerical modelling and microseismicity, 9th Int. Symposium of Landslides A.A. Balkema, Rio de Janeiro, pp. 481-487.

Einstein, H.H., Veneziano, D., Baecher, G.B., O'Reilly, K.J., 1983. The effect of discontinuity Persistence an Rock Slope Stability. Int. J. Rock Mech. Min. Sci. & Geomech. Abstr. 20, 227-236.

Erismann, T.H., Abele, G., 2001. Dynamics of Rockslides and Rockfalls. Springer, Berlind a.o.

Fischer, L., Huggel, C., 2008. Methodical Design for Stability Assessments of Permafrost-Affected High-Mountain Rock Walls. In: Kane, D.L., Hinkel, K.M. (Eds.), 9th Int. Conf. on Permafrost. INE-UAF, Fairbanks, Alaska, US, pp. 439-444.

Fischer, L., Huggel, C., Lemy, F., 2007. Investigation and modeling of periglacial rock fall events in the European Alps. Geophysical Research Abstracts 9, 08160.

Fischer, L., Kääb, A., Huggel, C., Noetzli, J., 2006. Geology, glacier retreat and permafrost degradation as controlling factors of slope instabilities in a high-mountain rock wall: the Monte Rosa east face. Nat. Hazards Earth Syst. Sci. 6, 761-772.

Fischer, L., Amann, F., Moore, J.R., Huggel, C., 2010. Assessment of periglacial slope stability for the 1988 Tschierva rock avalanche (Piz Morteratsch, Switzerland). Engineering Geology 116, 32-43.

Geertsema, M., Clague, J.J., Schwab, J.W., Evans, S.G., 2006. An overview of recent large catastrophic landslides in northern British Columbia, Canada. Engineering Geology 83, 120-143.

Glamheden, R., 2001. Thermo-Mechanical Behaviour of Refrigerated Caverns in Hard Rock. Chalmers University of Technology, Göteborg.

Goodman, R.E., 1970. The deformability of joints. In: Materials, A.S.T.a. (Ed.), Determination of the insitu Modulus of deformation of rock. Spec. Tech. Publications, pp. 174-196.

Gruber, S., Haeberli, W., 2007. Permafrost in steep bedrock slopes and its temperature-related destabilization following climate change. Journal of Geophysical Research - Earth Surface 112, F02S13.

Gruber, S., Hoelzle, M., Haeberli, W., 2004. Permafrost thaw and destabilization of Alpine rock walls in the hot summer of 2003. Geophys. Res. Lett. 31, L15054.

Günzel, F., 2008. Shear Strength of Ice-Filled Rock Joints. In: Kane, D.L., Hinkel, K.M. (Eds.), 9th Int. Conf. on Permafrost. INE-UAF, Fairbanks, Alaska, US, pp. 581-586.

Günzel, F., 2012. Shear strength of rock joints filled with frozen sand. In: Hinkel, K.M. (Ed.), 10th International Conference on Permafrost, Salekhard, Russia, pp. 143-148.

Haeberli, W., 1992. Construction, environmental problems and natural hazards in periglacial mountain belts. Permafrost and Periglac. Process. 3, 111-124.

Haeberli, W., 2005. Investigating glacier-permafrost relationships in high-mountain area: historical background, selected examples and research needs. In: Harris, C., Murton, J.B. (Eds.), Cryospheric Systems: Glaciers and Permafrost. Geological Society Special Publication, London, pp. 29-37.

Haeberli, W., Wegmann, M., Vonder Mühll, D., 1997. Slope stability problems related to glacier shrinkage and permafrost degradation in the Alps. Eclogae Geologicae Helvetiae 90, 407-414.

Haeberli, W., Huggel, C., Kääb, A., Polkvoj, A., Zotikov, I., Osokin, N., 2003. Permafrost conditions in the starting zone of the Kolka-Karmadon rock/ice slide of 20 September 2002 in North Ossetia (Russian Caucasus), 8th Int. Conf. on Permafrost, Zurich, Switzerland, pp. 49-50.

Haeberli, W., Huggel, C., Kääb, A., Zgraggen-Oswald, S., Polkvoj, A., Galushkin, I., Zotikov, I., Osokin, N., 2004. The Kolka-Karmadon rock/ice slide of 20 September 2002: an extraordinary event of historical dimensions in North Ossetia, Russian Caucasus. Journal of Glaciology 50, 533-546.

Hall, K., Thorn, C.E., Matsuoka, N., Prick, A., 2002. Weathering in cold regions: some thoughts and perspectives. Progress in Physical Geography 26, 577-603.

Hallet, B., 2006. Geology - Why do freezing rocks break? Science 314, 1092-1093.

Hallet, B., Walder, J.S., Stubbs, C.W., 1991. Weathering by segregation ice growth in microcracks at sustained sub-zero temperatures: verification from an experimental study using acoustic emissions. Permafrost and Periglacial Processes 2, 283-300.

Hasler, A., Talzi, I., Beutel, J., Tschudin, C., Gruber, S., 2008. Wireless Sensor Networks in Permafrost Research: Concept, Requirements, Implementation, and Challenges. In: Kane, D.L., Hinkel, K.M. (Eds.), 9th Int. Conf. on Permafrost. INE-UAF, Fairbanks, U.S., pp. 669-674.

Hoek, E., Brown, E.T., 1980. Empricial strength criterion for rock masses. J. Geotech. Engng Div. 106, 1013-1035.

Holm, K., Bovis, M., Jakob, J., 2004. The landslide response of alpine basins to post-Little Ice Age glaical thinning and retreat. Geomorphology 57, 201-216.

Huggel, C., 2009. Recent extreme slope failures in glacial environments: effects of thermal perturbation. Quaternary Science Reviews 28, 1119-1130.

Huggel, C., Caplan-Auerbach, J., Waythomas, C.F., Wessels, R.L., 2007. Monitoring and modelling ice-rock avalanches from ice-capped volcanoes: a case study of frequent large avalanches on Iliamna Volcano, Alaska. Journal of Volcanology and Geothermal Research 168, 114-136.

Huggel, C., Gruber, S., Caplan-Auerbach, J., Wessels, R.L., Molnia, B.F., 2008. The 2005 Mt. Steller, Alaska, Rock-Ice Avalanche: A Large Slope Failure in Cold Permafrost. In: Kane, D.L., Hinkel, K.M. (Eds.), 9th Int. Conf. on Permafrost. INE-UAF, Fairbanks, Alaska, US, pp. 747-752.

Inada, Y., Yokota, K., 1984. Some Studies of Low-Temperature Rock Strength. Int. J. Rock Mech. Min. Sci. 21, 145-153.

Indraratna, B., Welideniya, H.S., Brown, E.T., 2005. A shear strength model for idealised infilled joints under constant normal stiffness. Geotechnique 55, 215-226.

Irwin, G.R., 1958. Fracture. In: Flügge, S. (Ed.), Handbuch der Physik 6. Springer, Berlin, pp. 551-590.

Kemeny, J., 2003. The time-dependent reduction of sliding cohesion due to rock bridges along discontinuities: A fracture mechanics approach. Rock. Mech. Rock Eng. 36, 27-38.

Konrad, J.M., Morgenstern, N.R., 1982. Prediction of frost heave in the laboratory during transient freezing. Canadian Geotechnical Journal 31, 250-259.

Körner, H., Ulrich, R., 1965. Geologische und felsmechanische Untersuchungen für die Gipfelstation der Seilbahn Eibsee - Zugspitze. Geologica Bavarica 55, 404-421.

Korup, O., Clague, J.J., 2009. Natural hazards, extreme events, and moutain topography. Quaternary Science Reviews 28, 977-990.

Korup, O., Densmore, A.L., Schlunegger, F., 2010. The role of landslides in mountain range evolution. Geomorphology 120, 77-90.

Krautblatter, M., Dikau, R., 2007. Towards a uniform concept for the comparison and extrapolation of rockwall retreat and rockfall supply. Geografiska Annaler 89 A, 21-40.

Krautblatter, M., Hauck, C., 2007. Electrical resitivity tomography monitoring of permafrost in solid rock walls. Journal of Geophysical Research - Earth Surface 112, F02S20.

Krautblatter, M., Verleysdonk, S., Flores-Orozco, A., Kemna, A., 2010. Temperature-calibrated imaging of seasonal changes in permafrost rock walls by quantitative electrical resistivity tomography (Zugspitze, German/Austrian Alps). Journal of Geophysical Research-Earth Surface 115, F02003.

Krautblatter, M., Huggel, C., Deline, P., Hasler, A., 2012. Research perspectives for instable high-alpine bedrock permafrost: measurement, modelling and process understanding. Permafrost and Periglacial Processes 23, 80-88.

Krus, M., 1995. Feuchtetransport und Speicherkoeffizienten poröser mineralischer Baustoffe - theoretische Grundlagen und neue MeßtechnikenPh.D., University of Stuttgart, Stuttgart.

Li, N., Zhang, P., Chen, Y., Swoboda, G., 2003. Fatigue properties of cracked, saturated and frozen sandstone samples under cyclic loading. Int. J. Rock Mech. & Mining Sciences 40, 145-150.

Lipovsky, P., Evans, S., Clague, J., Hopkinson, C., Couture, R., Bobrowsky, P., Ekstrom, G., Demuth, M., Delaney, K., Roberts, N., Clarke, G., Schaeffer, A., 2008. The July 2007 rock and ice avalanches at Mount Steele, St. Elias Mountains, Yukon, Canada. Landslides 5, 445-455.

Matsuoka, N., 1990. Mechanisms of Rock Breakdown by Frost Action - an Experimental Approach. Cold Reg Sci Technol 17, 253-270.
Matsuoka, N., 2001. Direct Observation of Frost Wedging in Alpine Bedrock. Earth Surf. Process. Landforms 26, 601-614.
Matsuoka, N., Murton, J., 2008. Frost weathering: Recent advances and future directions. Permafrost and Periglacial Processes 19, 195-210.
McColl, S.T., 2012. Paraglacial rock-slope stability. Geomorphology, 1-16.
Mellor, M., 1973. Mechanical Properties of Rocks at Low Temperatures, 2nd Int. Conference on Permafrost, Yakutsk, Russia, pp. 334-344.
Messerli, B., 2006. From nature-dominated to human-dominated global environmental change in the mountains of the world. In: Price, M.F. (Ed.), Global Chnage in Mountain Regions. Sapiens Publishing, Duncow, pp. 3-5.
Miller, H., 1961. Der Bau des westlichen Wettersteingebirges. Z. dt. geol. Ges. 113, 409-425.
Murton, J.B., Peterson, R., Ozouf, J.C., 2006. Bedrock fracture by ice segregation in cold regions. Science 314, 1127-1129.
Murton, J.B., Coutard, J.-P., Lautridou, J.P., Ozouf, J.-C., Robinson, D.A., Williams, R.B.G., Guillemet, G., Simmons, P., 2000. Experimental design for a pilot study on bedrock weathering near the permafrost table. Earth Surf. Process. Landforms 25, 1281-1294.
Nixon, J.F., 1982. Frost heave predictions using the segregation potential concept Canadian Geotechnical Journal 19, 526-529.
Noetzli, J., Gruber, S., 2009. Transient thermal effects in Alpine permafrost. The Cryosphere 3, 85-99.
Noetzli, J., Hoelzle, M., Haeberli, W., 2003. Mountain permafrost and recent Alpine rock-fall events: a GIS-based approach to determine critical factors. In: Phillips, M., Springman, S., Arenson, L. (Eds.), 8th International Conference on Permafrost. Swets & Zeitlinger, Zurich.
Paterson, W.S.B., 2001. The Physics of Glaciers. Butterworth & Heinemann, Oxford.
Patton, F.D., 1966. Multiple modes of shear failure in rock, 1st Congress Int. Society for Rock Mech. Lab. of Civil Engineering, Lisbon, Portugal, pp. 509-513.
Pogrebiskiy, M.I., Chernyshev, S.N., 1977. Determination of the Permeability of the Frozen Fissured Rock Massif in the Vicinity of the Kolyma Hydroelectric Power Station. Cold Regions Research and Engineering Laboratory - Draft Translation 634, 1-13.
Prager, C., Zangerl, C., Patzelt, G., Brandner, R., 2008. Age distribution of fossil landslides in the Tyrol (Austria) and its surrounding areas. Natural Hazards and Earth System Sciences 8, 377-407.
Prick, A., 1997. Critical degree of saturation as a threshold moisture level in frost weathering of limestones. Permafrost and Periglacial Processes 8, 91-99.
Rabatel, A., Deline, P., Jaillet, S., Ravanel, L., 2008. Rock falls in high-alpine rock walls quantified by terrestrial lidar measurements: A case study in the Mont Blanc area. Geophys. Res. Lett. 35, L10502.
Ravanel, L., Deline, P., 2008. La face ouest des Drus (massif du Mont-Blanc). Évolution de l'instabilité d'une paroi rocheuse dans la haute montagne alpine depuis la fin du petit age glaciaire. Geomorphologie 4, 261-272.
Renshaw, C.E., Schulson, E.M., 2001. Universal behaviour in compressive failure of brittle materials. Nature 412, 897-900.
Sanderson, T., 1988. Ice mechanics and risks to offshore structures. Springer, Amsterdam.

Sass, O., 2005. Rock moisture measurements: Techniques, results, and implications for weathering. Earth Surf. Process. Landforms 30, 359-374.

Sass, O., Krautblatter, M., Morche, D., 2007. Rapid lake infill following major rockfall (bergsturz) events revealed by ground-penetrating radar (GPR) measurements, Reintal, German Alps. Holocene 17, 965-976.

Schulson, E.M., Duval, P., 2009. Creep and fracture of ice. University Press, Cambridge.

Slaymaker, O., 2009. Proglaical, periglacial or paraglacial? In: Knight, J., Harrison, S. (Eds.), Periglacial and Paraglacial Processes and Environments. Geological Society Special Publications, London, pp. 268-288.

Sosio, R., Crosta, G.B., Hungr, O., 2008. Complete dynamic modeling calibration for the Thurwieser rock avalanche (Italian Central Alps). Engineering Geology 100, 11-26.

Tang, G.Z., Wang, X.H., 2006. Modeling the thaw boundary in broken rock zones in permafrost in the presence of surface water flows. Tunnelling and Underground Space Technology 21, 684-689.

Terzaghi, K., 1962. Stability of steep slopes in hard unweathered rock. Geotechnique 12, 251-270.

Tharp, T.M., 1987. Conditions for crack propagation by frost wedging. Geol. Soc. Am. Bull. 99, 94-102.

Ulrich, R., King, L., 1993. Influence of mountain permafrost on construction in the Zugspitze mountains, Bavarian Alps, Germany, 6th Int. Conf. on Permafrost, Bejing, pp. 625-630.

Walder, J., Hallet, B., 1985. A Theoretical-Model of the Fracture of Rock During Freezing. Geol. Soc. Am. Bull. 96, 336-346.

Weertman, J., 1973. Creep of ice. In: Whalley, E., Jones, S.J., Gold, L.W. (Eds.), Physics and Chemistry of Ice. Royal Soc. of Canada, Ottawa, pp. 320-337.

Wegmann, M., Gudmundsson, G.H., Haeberli, W., 1998. Permafrost changes in rock walls and the retreat of Alpine glaciers: a thermal modelling approach. Permafrost and Periglac. Process. 9, 23-33.

Whalley, W.B., 1982. Crack propagation and associated weathering in igneous rocks. Z. Geomorph. 26, 33-54.

Whalley, W.B., 1984. Rockfalls. In: Brunsden, D., Prior, D.B. (Eds.), Slope Instability. Wiley & Sons, Chichester, pp. 217-256.

Whalley, W.B., Bruce, B.R., Rainey, M.M., 2004. Weathering, blockfields, and fracture systems and the implications of long-term landscape formation: some evidence from Lingen and Oksforddjokelen areas in North Norway. Polar Geography 28, 93-119.

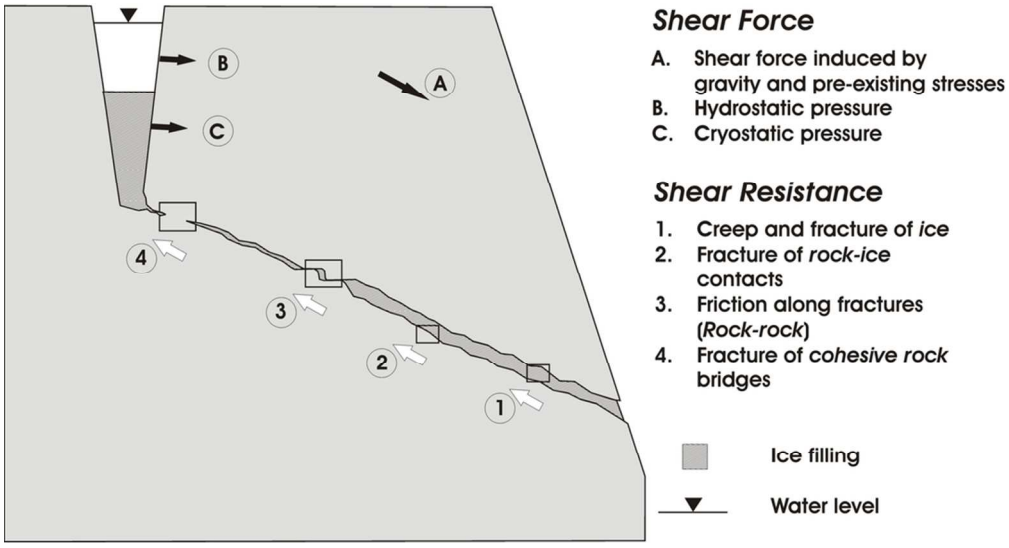

A schematic representation of the rock-ice mechanical model
91x49mm (300 x 300 DPI)

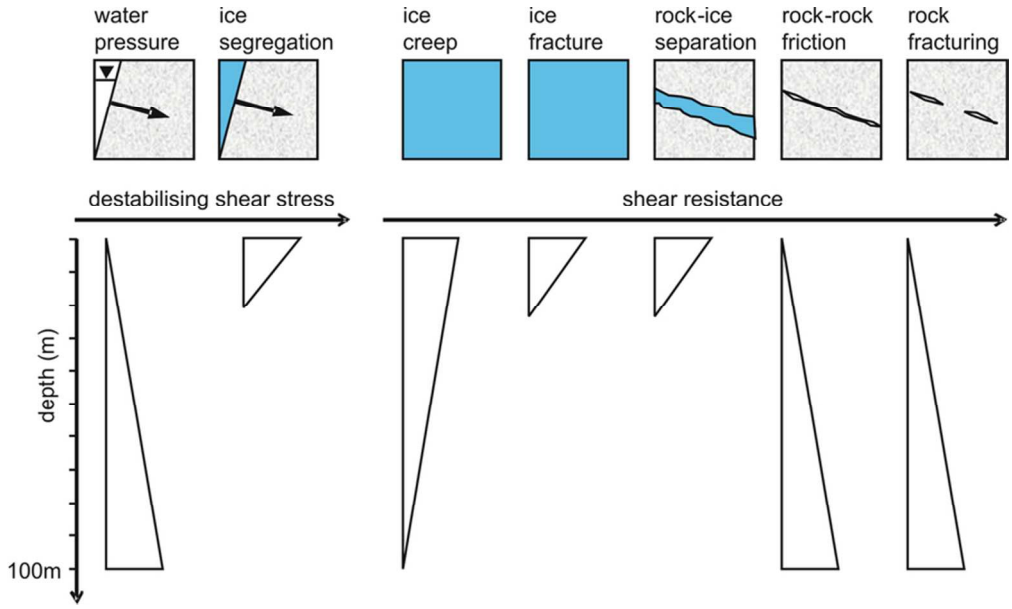

The efficiency of shear force and shear resistance with depth of the shear plane.
75x45mm (300 x 300 DPI)

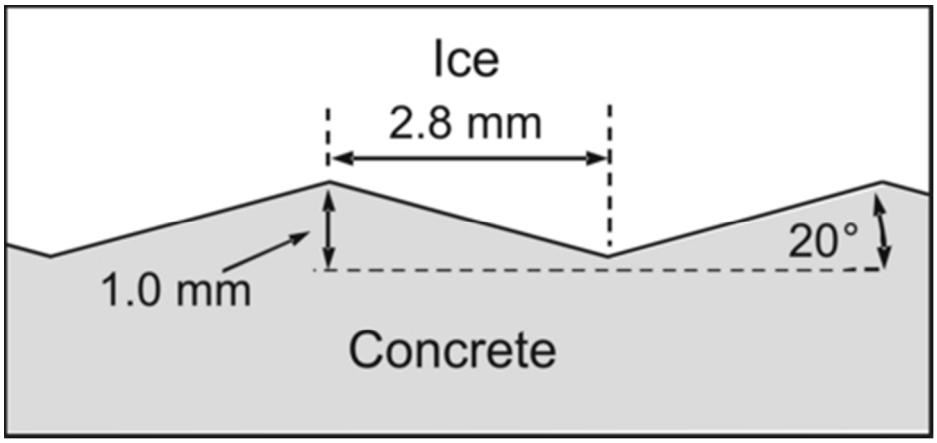

Dimensions of the saw-tooth surface
39x18mm (300 x 300 DPI)

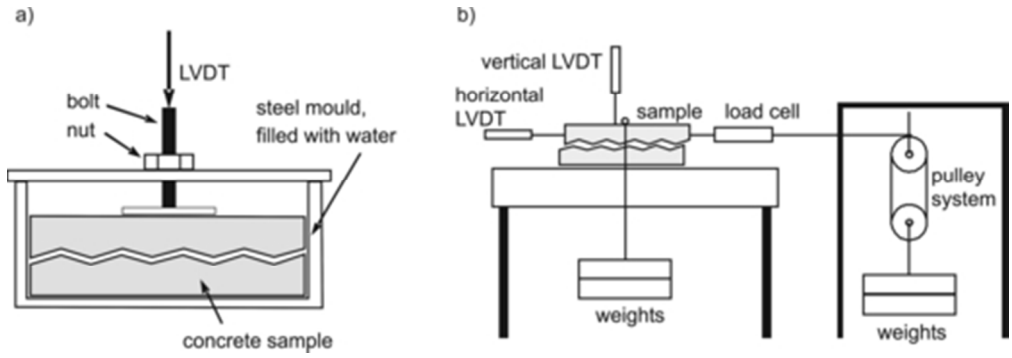

a) Preparation of sandwich sample; b) Schematic overview over experimental set-up of the constant stress tests
43x15mm (300 x 300 DPI)

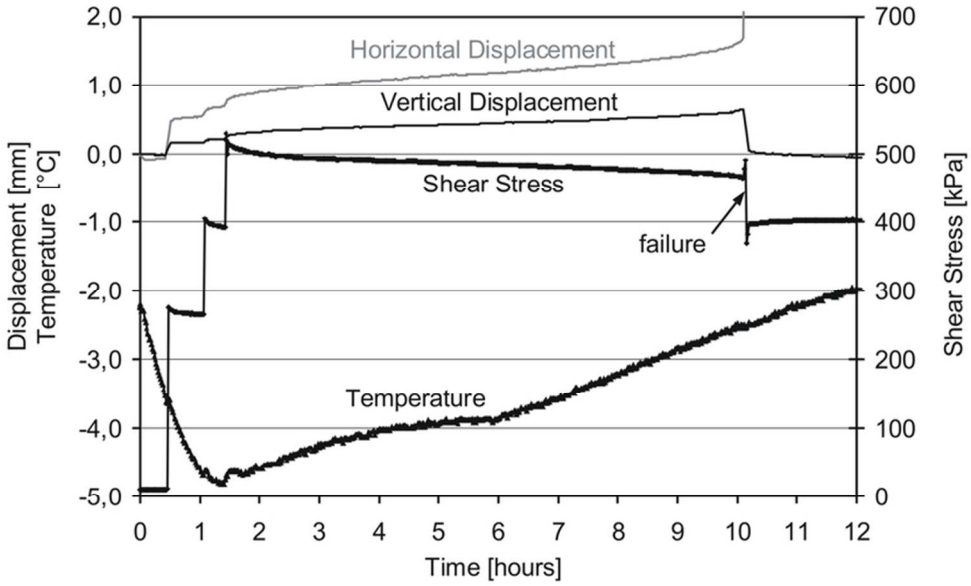

Results of a constant stress experiment (concrete-ice sample, normal stress = 207 kPa) plotted against time.
72x44mm (300 x 300 DPI)

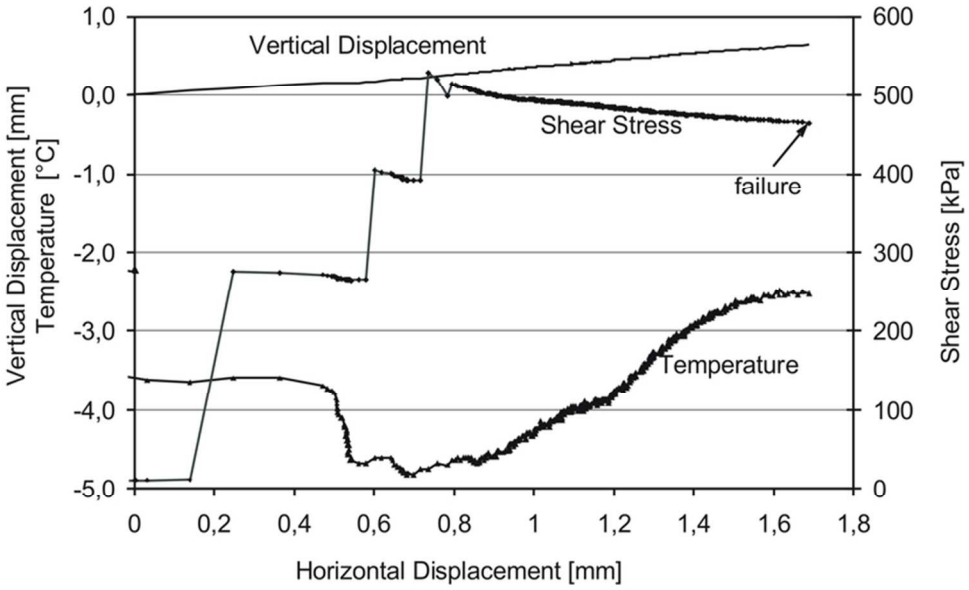

Results of a constant stress experiment (concrete-ice sample, normal stress = 207 kPa) plotted against horizontal displacement.
72x44mm (300 x 300 DPI)

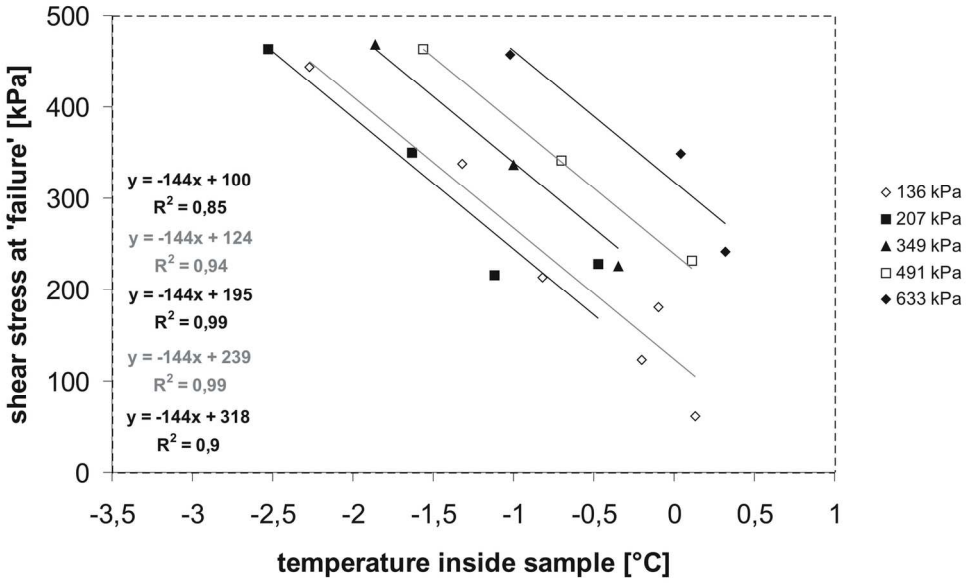

Shear stress at failure plotted against failure temperature for constant-stress tests with concrete-ice samples.
75x47mm (600 x 600 DPI)

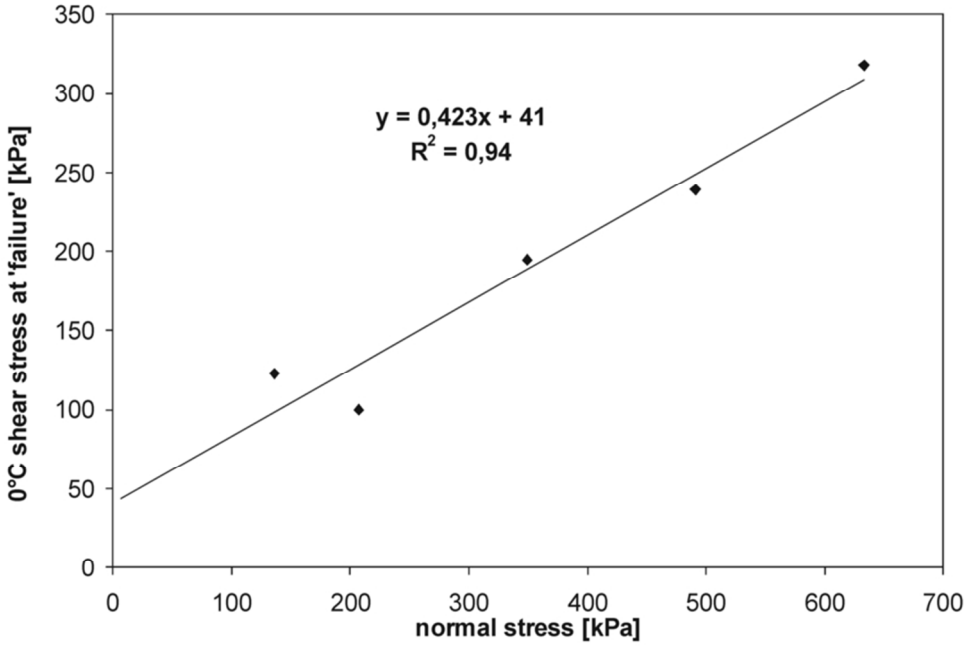

Linear relationship of shear stress at failure vs. normal stress for constant stress tests for 0°C.
77x51mm (300 x 300 DPI)

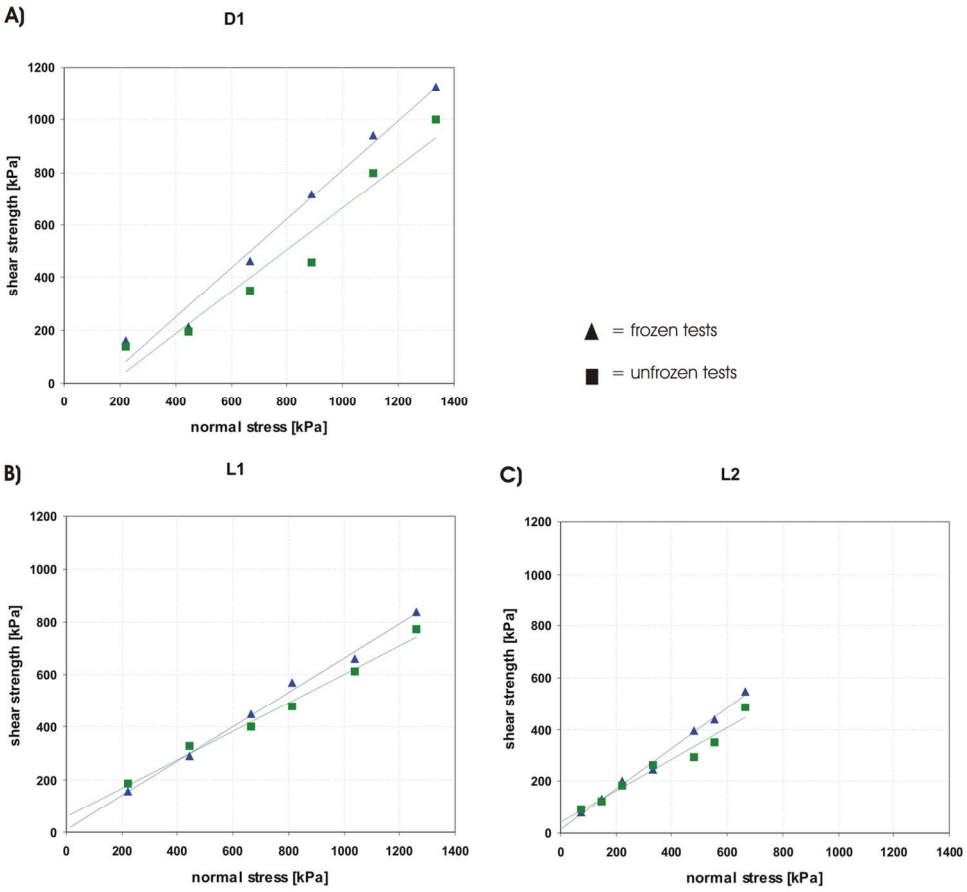

Peak shear strength – normal stress relationships for direct shear tests on the dolomite sample (D1) and limestone samples (L1, L2) performed with constant velocities.
136x125mm (300 x 300 DPI)